

## AN EXPERIMENTAL AND NUMERICAL INVESTIGATION ON THE LOW-VELOCITY IMPACT RESPONSE OF NANO- REINFORCED POLYPROPYLENE CORE SANDWICH STRUCTURES

M. Bagheri Tofighi,<sup>1</sup> H. Biglari,<sup>1\*</sup> and M. M. Shokrieh<sup>2</sup>

**Keywords:** low-velocity impact, Johnson–Cook material model, sandwich structure, polypropylene, finite-element model

*The impact behavior of sandwich structures was studied using experimental and numerical methods. Polypropylene with 0.5 wt% of graphene (PP/0.5% G) or pure polypropylene (PP) was sandwiched between aluminum face sheets for experimental tests. Impact tests revealed that the nanoreinforced structures had a higher contact force and a shorter contact duration than pure core structures. Both the damage area and the dent depth were lower for nano-reinforced structures. More energy absorbed the pure structures. The higher absorbed energy can be explained by the higher amount of damage that occurred in the structure. To further investigate the impact response of the sandwich structures, a three-dimensional quarter model was developed and implemented in the ABAQUS software. The strain-rate-dependent behavior of the core and face sheets was investigated using the Johnson–Cook material model to simulate the impact behavior of aluminum, PP, and G/PP layers. Simulation results were compared with experimental data, and a good agreement between them was found to exist. The validated finite-element model was used for studying the effects of geometrical and material parameters, including the thickness of aluminum and PP layers, different weight ratios of nanoparticles, and different mechanical properties of the aluminum layers, on the impact response of sandwich structures. By introducing graphene up to 0.5 wt% into the PP material, all of the impact outputs reached their extremum amounts, which were considerably affected by the yield strength and elastic modulus of aluminum layers.*

---

<sup>1</sup>Department of Mechanical Engineering, University of Tabriz, 29 Bahman Blvd, Tabriz, 51666-16471, Iran

<sup>2</sup>Composites Research Laboratory, Center of Excellence in Experimental Solid Mechanics and Dynamics, School of Mechanical Engineering, Iran University of Science and Technology, Tehran, 16846-13114, Iran

\*Corresponding author; e-mail: hbiglari@tabrizu.ac.ir

## 1. Introduction

Using hybrid materials in sandwich structures have made it possible to reveal the particular characteristics of the different materials in the final structure. Furthermore, multilayer structures have a higher resistance to the fatigue and impact actions due to the more plastic energy dissipation in them than in monolithic ones. Multilayer laminates, including metal-metal and polymer-metal composites, are widely used in aerospace and automotive industries. These structures are often subjected to impact actions. Therefore, it is necessary to investigate their impact behavior carefully [1-3].

Riccio et al. [4] added different micro- and nanoparticles to the polypropylene core of sandwich structures and studied their effect on the low-velocity impact behavior of sandwich configurations. Bulut [5] examined the low-velocity impact performance of polypropylene-core-based sandwich composites to assess the effect of facesheet thickness on their mechanical responses. Hosur et al. [6], for the first time, studied the low-velocity impact response of nanophase foam core sandwich composites. They added nanoclay particles to the polyurethane core of a sandwich panel and studied their effect on the impact damage experimentally. Hosur et al. [7] also introduced nanoclay particles into both face sheets and core of sandwich panels and checked the impact response of final structures. In another study, Hosur et al. [8] conducted several impact tests on sandwich panels to study the effect of nanoclay on their impact outputs, including the contact force, contact duration, displacement, and dissipated energy. Bhuian et al. [9] considered different weight percentages of carbon nanofibers as reinforcements of a sandwich panel with a polyurethane core. The sandwich panel with 0.2% carbon nanofibers dissipated more impact energy than those with other weight percentages. Avila et al. [10] created sandwich panels with a polystyrene core and fiber-glass/nano-modified epoxy face sheets. They classified the impact damage of the panels into six categories, including (i) barely visible damages; (ii) sub-critical damage, i.e., cracked face sheet and core; (iii) tearing of upper face sheets and core crushing; (iv) debonding of the lower face sheet and core; (v) cracking of the lower face sheet; (vi) tearing and perforation of the lower face sheet. Reis et al. [11] fabricated glass fiber/epoxy resin sandwich composite specimens with a core of balsa wood. The face sheets were fabricated in both pure and nanoreinforced conditions. The nanoenhanced sandwich plates presented higher maximum impact loads, lower displacements, the best performance in terms of the elastic recuperation, and the maximum residual flexural strength. Taraghi and Fereidoon [12] performed experimental low-velocity impact tests to study the effect of multiwalled carbon nanotubes (MWCNTs) on the internal and external damage of foam core sandwich panels with Kevlar-fiber-reinforced epoxy face sheets.

Ramakrishnan et al. [13] explored the effect of adding M52N nanostrength copolymer triblocks on the low-velocity impact of sandwich panels with Kevlar facesheets and a Rohacell foam core. They developed a numerical model in an explicit LS-Dyna FE software, and a constitutive law based on the continuum damage mechanics was used to simulate composite facesheets with and without nanoreinforcements. The input parameters related to the stiffness and strength of the composite were obtained by conducting a set of mechanical characterization tests. Feli and Jalilian [14] presented a three-dimensional solution based on Fourier's series and the Generalized Differential Quadrature (GDQ) method to model the impact on sandwich panels with nanostructured face sheets. They verified their theoretical model against impact experiments. Salami [15] presented a theoretical analysis based on the Extended High Order Sandwich Panel Theory to study the impact behavior of nanoreinforced sandwich structures. Three different configurations including a uniformly distributed (UD) case and two different functionally graded (FG) cases FG-V and FG- $\Lambda$  were considered for the distribution of carbon nanotubes in face sheets. The sandwich beam with FG-V face sheets showed the highest contact force and the lowest deflection among the different configurations.

Nowadays, to decrease the weight of mechanical parts, the employment of lightweight materials, such as polymers is constantly increasing [16]. Polypropylene, as a kind of thermoplastic polymers, is widely used in packaging, automotive, and aerospace industries. Polypropylene is a low-density polymer with outstanding electrical and mechanical characteristics. It is used in indoor panels of automobiles because of its recyclability. Ku et al. [17] studied the surface treatment of polypropylene specimens to improve the bonding strength of polypropylene to aluminum plates. At the time of writing of this paper, there were no studies in the literature on the finite-element modeling of neat and nanoreinforced aluminum/polypropylene/aluminum plates under low-velocity impact loadings. Most of previous investigations into the nanostructured sandwich plates were performed experimentally or analytically. In the present study, graphene nanoparticles were used as the reinforcement of the core

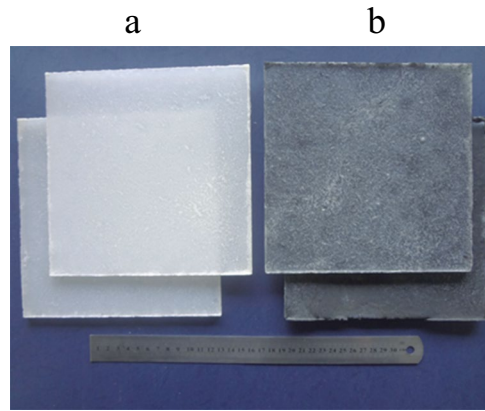


Fig. 1. Pure (a) and 0.5% graphene-reinforced (b) PP plates.

material of aluminum/PP/aluminum (AL/PP/AL) sandwich plates. The core material was modeled using the Johnson–Cook material model. The Johnson–Cook parameters were obtained by using an innovative method [18]. In the present manuscript, it is examined if the Johnson–Cook material constants are appropriate for simulating the strain-rate-dependent behavior of a nanoreinforced PP.

## 2. Experimental Work

Low-velocity impact tests were conducted on both pure and nanoreinforced AL/PP/AL sandwich structures to investigate the effects of adding nanoparticles and different loading conditions on their impact outputs.

### 2.1. Raw materials

Polypropylene was provided from Shazand Petrochemical Corporation (Arak) in a powder form. Nanographene platelets were obtained from API Technology Pioneers. The nanoplatelets had a maximum number of plates across the thickness and maximum dimensions of 10 and 45  $\mu\text{m}$ , respectively. Aluminum 1050-H14 was supplied in a plate form of dimensions of  $1 \times 2$  m and of thickness of 1 mm. A two-component Megapox™ epoxy adhesive was used in the current experimental study.

### 2.2. Manufacture of pure and graphene-reinforced PP plates

The main operations in the production of nanoreinforced polypropylene were sonication and mechanical stirring. Graphene particles were diffused in alcohol by using the main operations simultaneously for 30 min. In the next stage, PP particles were added. The main operations were repeated again for 30 min. The final blend was decanted into a square mold with desired dimensions. The mold was placed in an oven with a temperature of 250°C for melting the PP particles. The G/PP plates were prepared after cooling the mold content. Figure 1 shows the pure and 0.5 wt% graphene-reinforced PP plates. A low weight fraction of graphene was used to reduce its agglomeration. Shokrieh and Joneidi [18] showed that the best enhancement of the impact strength is reached at 0.5 wt% graphene. Adding a higher amount of graphene did not improve the impact response of nanoreinforced polypropylene.

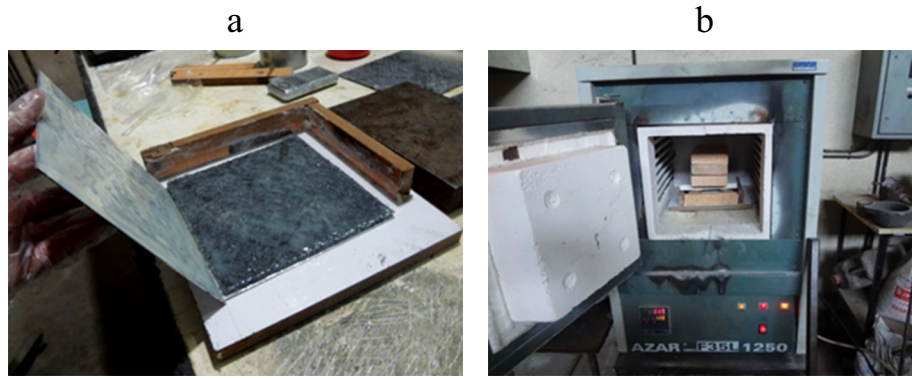


Fig. 2. Fabrication of AL/PP/AL sandwich structures: (a) Coating internal surfaces with an adhesive and (b) the frame with its contents in an oven.

TABLE 1. Low-Velocity Impact Test Scheme for AL/PP/AL Structures

Test number	Core (pure or nano-reinforced)	Height, cm	Mass, kg	Energy, J	Velocity, m/s	Linear momentum, kg·m/s
1	Pure	25	2.7	6.6	2.2	5.94
2	Nanoreinforced	25	2.7	6.6	2.2	5.94
3	Pure	57.4	2.7	15.2	3.35	9.04
4	Nanoreinforced	57.4	2.7	15.2	3.35	9.04
5	Pure	25	6.2	15.2	2.2	13.64
6	Nanoreinforced	25	6.2	15.2	2.2	13.64

### 2.3. Surface treatment of aluminum and PP plates

Adhesively bonded joints were used for producing sandwich structures. The surface treatment was performed for both aluminum and PP surfaces to reach a powerful and firm connection between the aluminum and PP layers. All surfaces of PP and G/PP were scratched to promote the flow of adhesive into the polypropylene material. A chemical compound named Aston was utilized for cleaning aluminum faces. The FPL etch method according to [19] was used to ensure the removing of impurities from aluminum surfaces. The aluminum laminates were used just after their surface treatment to prevent them from becoming dirty.

### 2.4. Fabrication of AL/PP/AL sandwich structures

Thin wires were used as spacers between the aluminum and PP layers. Diameter of the wires was 0.4 mm, because the adhesive layer thickness was considered to be 0.4 mm for experimental specimens. A wooden frame was built for fixing the sliding movement of the aluminum and PP layers before curing the adhesive. A silicone gel with styling cream was used as lubricants on the frame surface to prevent the adhesion between the mold and the sandwich structure during the adhesive curing process. A resin/hardener weight ratio of 10/8 was used for the Megapox™ adhesive for bonding the aluminum to PP surfaces. Finally, the wooden frame was completed and additional weights were added on the sandwich structure. The mold with all contents was put in an oven at 120°C temperature for 2 h for a rapid curing of adhesive. The different steps involved in the production of AL/PP/AL sandwich structures are shown in Fig. 2.

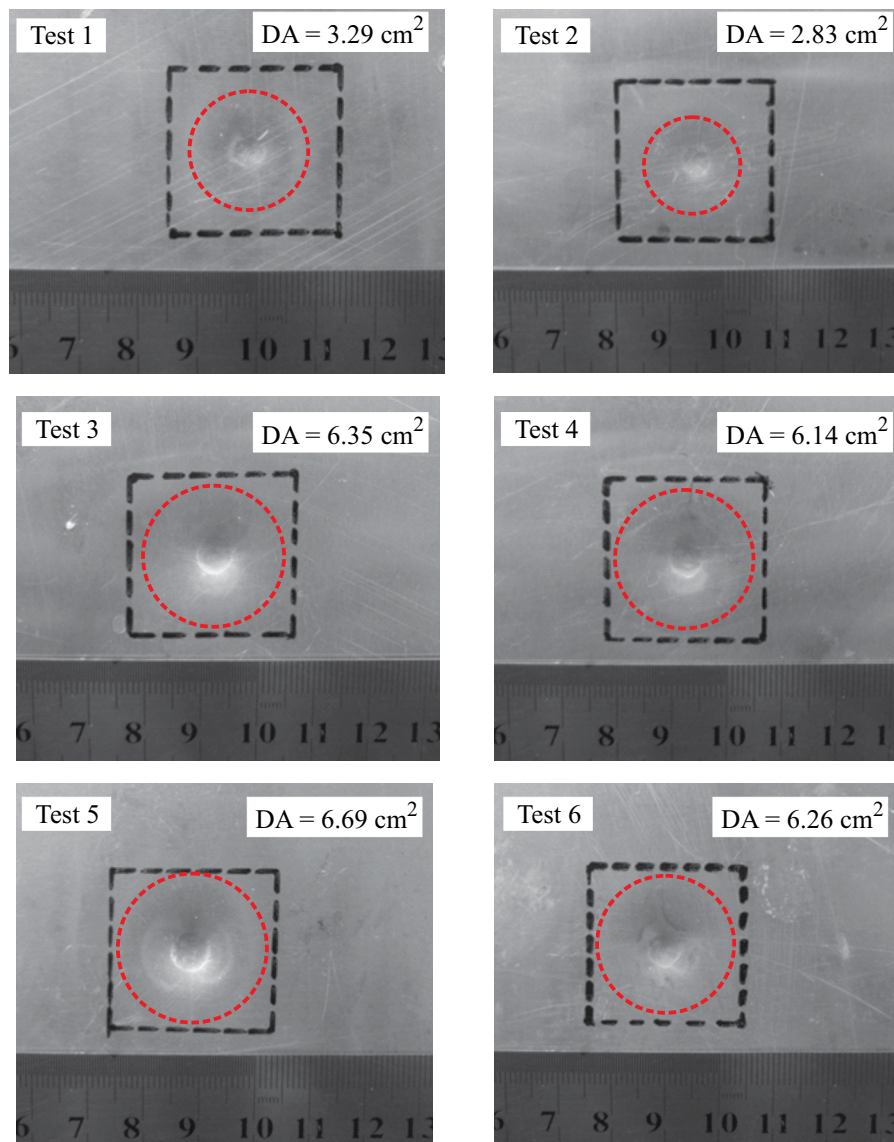


Fig. 3. The damaged area DA on the front face of pure and nanoreinforced core sandwich structures at different impact loading conditions according to Table 1.

## 2.5. Low-velocity impact tests

Several impact tests were performed using a drop weight test tower to study the low-velocity impact behavior of sandwich AL/PP/AL structures with pure and nanoreinforced cores. A square opening of 15-cm side in the middle of the sandwich structures was considered as the exposed surface of the target against the impact. The remaining width of the side was held using clamps.

The low-velocity impact test scheme is presented in Table 1. Hemispherical rigid impactors with an 8.1-mm radius with different masses and velocities, according to Table 1, were used. Test number (1, 2), (3, 4), and (5, 6) were considered as the paired experiments with the same impactor characteristics, but for different core materials (pure or nanoreinforced).

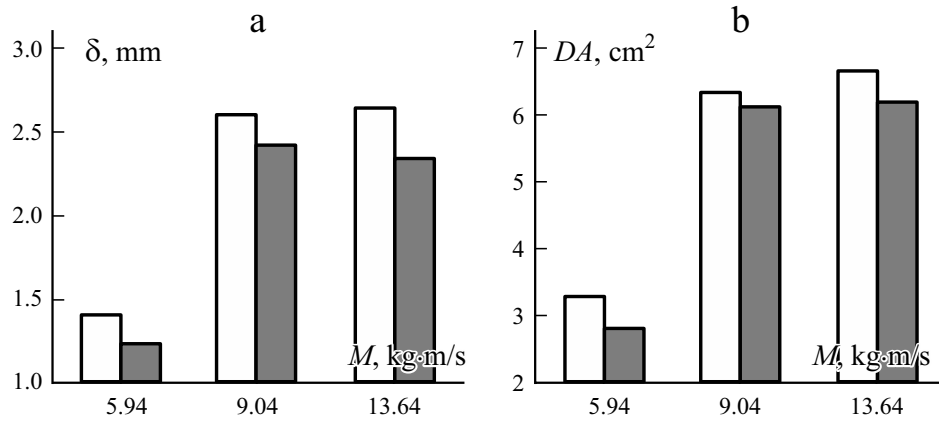


Fig. 4. Dent depth  $\delta$  and damaged area  $DA$  of the pure (□) and nanoreinforced-core (■) sandwich structures at different linear momentums  $M$  according to Table 1.

## 2.6. Impact test results

After the low-velocity impact tests, their results were determined. The acceleration–time diagrams were plotted by using an accelerometer located just behind the impactor. The contact force was obtained multiplying the acceleration by the impactor mass. The contact duration was considered as the total time of the acceleration–time diagram. An image processing software [20] (ImageJ) was used to measure the damage area on the front face and the maximum permanent transverse displacement of front and back faces. The impacted specimens were cut for measuring their transverse displacements. The maximum permanent transverse displacement of the front face was considered as the dent depth of the target structure. The damage area  $DA$  was considered as a circular deformed area just in the center of the front face. The radius of the damage area was assumed to be equal to the permanent plastic radius  $PR$ . The plastic radius was related to the damage area by the relation  $DA = \pi (PR)^2$ . Determining the plastic radius was difficult, because the damage area was expanded in the center of the face, but the radius of the dent area was distinguished visually in the software. Therefore, first the dent radius was determined visually, and the plastic radius was assumed four times of the dent radius for all tests. The remaining velocity of the impactor was calculated by subtracting the area under the curve of acceleration from the initial velocity of impactor. Then, the remaining kinetic energy of the impactor was calculated using the remaining velocity of impactor.

Figure 3 shows the damaged area on the front face of pure and nanoreinforced core sandwich structures for different impact masses and velocities. The damage area is quantified in Fig. 3 by using dotted circular boxes. According to Fig. 3, the damaged area was smaller for nano-reinforced core sandwich structures, but increased with increasing impact energy.

According to Fig. 4, the dent depth and the damaged area were greater for sandwich structures with a pure PP core in comparison with that of the sandwich structure a 0.5% graphene-reinforced PP core.

It should be noted that each experimental test was repeated three times. The average value of three quantities was reported as the final experimental output. The scattering of experimental data was reported for the contact force and the contact duration in Fig. 5. The same procedure was undertaken for other impact outputs. As shown in Fig. 5, comparing the repeated outputs for neat and nanoreinforced PP cases revealed that none of the impact outputs of nano-reinforced specimens were in the range of the impact outputs for pure specimens. For example, the maximum amount of the contact force for Test 1 (pure specimens) occurred in a repeat 1 equal to 4.22 kN. The minimum amount of the contact force for Test 2 (nanoreinforced specimens) occurred in a repeat 1 equal to 4.41 kN. This means that, even in the worst case, the contact force for nano-reinforced specimens was higher than the contact force for the pure specimen. This fact was observed in all cases and all impact outputs, except for some rare cases. For example, in Fig. 5b, the contact duration for Test 2-Repeat 1 condition was more than that for Test 1-Repeat 3. However, the average contact duration for Test 1 greater than for Test 2.

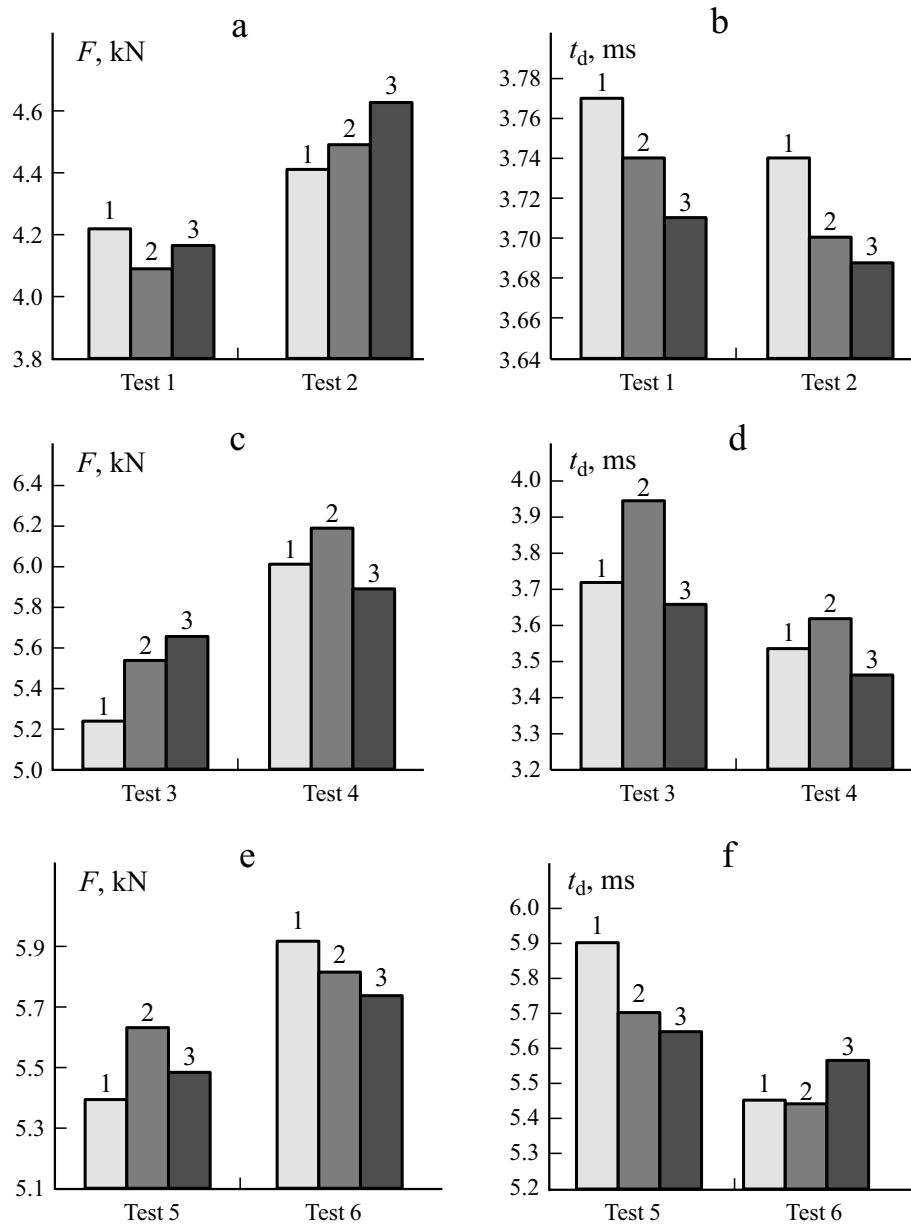


Fig. 5. Scattering of experimental data for the contact force  $F$  and contact duration  $t_d$  of outputs: (a)  $F$  in tests 1 and 2, (b)  $t_d$  in tests 1 and 2, (c)  $F$  in tests 3 and 4, (d)  $t_d$  in tests 3 and 4, (e)  $F$  in tests 5 and 6, and (f)  $t_d$  in tests 5 and 6. Numbers under the diagrams correspond the repeat number.

### 3. Finite-element modeling

Finite-element analyses were carried out to simulate the impact behavior of the sandwich composites. The effects of the strain rate and adding of nanoparticles were considered for nano-reinforced PP layers. The Johnson–Cook model parameters for the nanoreinforced PP material were characterized previously in [18] by using a strain-rate-dependent micromechanics model (SRDM). In the current study, the Johnson–Cook material constants were examined to simulate the low-velocity impact behavior of G/PP layers to check the efficiency of using these parameters to simulate the strain-rate-dependent behavior of G/PP materials in drop weight impact loadings. Although the present-finite element model was based on previous studies, some

explanations of the equations were provided here to allow a knowledgeable practitioner or expert to reproduce the results. The constitutive equation of polymers (Goldberg), the Halpin–Tsai micromechanics model, the constitutive equation of polymers filled with nanoparticles (SRDM), and the way of extracting the Johnson–Cook material model parameters of PP and G/PP are presented briefly in the following sections. Then, the material model for the adhesive layer and the detail of the three-dimensional finite-element model are explained. Afterwards, the numerical results are presented and compared with experimental outputs. Finally, the effects of different parameters, including the thickness of the aluminum and PP layers, the different weight ratio of nanoparticles, and the different mechanical properties of the aluminum layers, are simulated and discussed on the basis of the validated finite-element modeling process.

### 3.1. Constitutive equation of polymers

The Goldberg model [21] was introduced to predict the mechanical behavior of pure polymers. Goldberg stated that the stress field of the polymers can be calculated from strain fields. The inelastic strain was defined as

$$\dot{\varepsilon}_{ij}^I = 2D_0 \exp \left[ -\frac{1}{2} \left( \frac{Z}{\sigma_e} \right)^{2n} \right] \left( \frac{S_{ij}}{2\sqrt{J_2}} + \alpha \delta_{ij} \right), \quad (1)$$

where  $\dot{\varepsilon}_{ij}^I$  is the inelastic strain rate tensor which is defined as a function of the deviatoric stress  $S_{ij}$ , the second invariant  $J_2$  of deviatoric stress tensor and the state variables  $Z$  and  $\alpha$ , the maximum inelastic strain rate  $D_0$ , and the rate sensitivity  $n$  of the material. The effective stress  $\sigma_e$  is defined as

$$\sigma_e = \sqrt{3J_2} + \sqrt{3}\alpha\sigma_{kk}, \quad (2)$$

where  $\sigma_{kk}$  is the sum of normal stresses, which are equal to three principal stress. The state variables  $Z$  and  $\alpha$  are presented as

$$\dot{Z} = q(Z_1 - Z)\dot{\varepsilon}_e^I, \quad (3)$$

$$\dot{\alpha} = q(\alpha_1 - \alpha)\dot{\varepsilon}_e^I, \quad (4)$$

$$\dot{\varepsilon}_e^I = \sqrt{\frac{2}{3}} \dot{\varepsilon}_{ij}^I \dot{\varepsilon}_{ij}^I, \quad (5)$$

$$\dot{\varepsilon}_{ij}^I = \dot{\varepsilon}_{ij}^I - \frac{\dot{\varepsilon}_{kk}^I}{3} \delta_{ij}, \quad (6)$$

where  $q$  is the hardening rate effect of the material;  $Z_1$ ,  $\alpha_1$  and  $Z_0$ ,  $\alpha_0$  are the maximum and initial values of  $Z$  and  $\alpha$ , respectively. The term  $\dot{\varepsilon}_e^I$  is the effective deviatoric inelastic strain rate. The procedure of determining the material parameters, including  $D_0$ ,  $n$ ,  $Z_1$ ,  $Z_0$ ,  $\alpha_1$ ,  $\alpha_0$ , and  $q$  is described in [21]. Using the Goldberg model, stress–strain curves of the neat polypropylene were found by Shokrieh and Joneidi [18].

### 3.2. The Halpin–Tsai micromechanics model

The mechanical properties of composites were predicted in different studies by using different micromechanical methods, including Halpin–Tsai, Mori–Tanaka, Nielsen, etc. ones. The elastic modulus of the nanophased polymer was predicted by combining the mechanical properties of the polymer and nanoparticles. Equations of the Halpin–Tsai model [22] are

$$\frac{E}{E_m} = \frac{3}{8} \frac{1 + 2(l/d)\eta\nu_f}{1 - \eta\nu_f} + \frac{5}{8} \frac{1 + 2\eta\nu_f}{1 - \eta\nu_f}, \quad (7)$$



TABLE 2. Material Parameters of the Aluminum, Pure PP, and G/PP Layers [18]

Material	$\rho$ , kg/m <sup>3</sup>	$E$ , GPa	$\nu$	$A$	$B$	$n$	$C$
				MPa			
PP	900	1.071	0.4	23	33.86	0.544	0.0643
PP/ 0.5% G	900	1.305	0.4	23.065	49.74	0.6309	0.0719
PP/ 1% G	900	1.061	0.4	23.03	46.25	0.5867	0.0668
PP/ 2% G	900	0.92	0.4	23.01	30.83	0.3911	0.0445
Aluminum 1050-H14	2710	71	0.33	102	97	0.18	0.01

$$\eta = \frac{(E_f / E_m) - (d / 4t)}{(E_f / E_m) + (d / 2t)}, \quad (8)$$

where  $E$ ,  $E_m$ , and  $E_f$  are the tangential elastic moduli of composite, polymeric matrix, and the reinforcement, respectively;  $\nu_f$  is the reinforcement volume fraction, and  $l$  and  $d$  are the average length and diameter of the reinforcement particle, respectively.

### 3.3. Strain-rate-dependent micromechanics model (SRDM model)

Shokrieh et al. [22] introduced a strain-rate-dependent micromechanics model (SRDM model) as a constitutive equation for nanoreinforced polymers to predict the stress–strain behavior of nanophased polymers at different strain rates.

The SRDM model is a combination of Goldberg and Halpin–Tsai models. Shokrieh and Joneidi [18] plotted the stress–strain curves of PP at different strain rates using the Goldberg model and the stress–strain curves of G/PP at different strain rates.

### 3.4. Characterization of the Johnson–Cook material model as an input of FEM

The stress–strain curves of PP and G/PP at different strain rates were prerequisites for determining the Johnson–Cook parameters. The strain-rate-dependent behavior of PP and G/PP was simulated by the Johnson–Cook material model [18]. The Johnson–Cook parameters were used in the equation

$$\sigma = [A + B\varepsilon_p^n] [1 + C \ln(\dot{\varepsilon}^*)], \quad (9)$$

where  $A$ ,  $B$ ,  $C$ , and  $n$  are material constants:  $A$  is the yield strength at the reference strain rate;  $B$  and  $n$  are the strain hardening coefficients; the  $C$  is the strain-rate-sensitivity coefficient. The parameters  $\dot{\varepsilon}^*$ ,  $\sigma$ , and  $\varepsilon_p$  are the dimensionless plastic strain rate, flow stress, and equivalent plastic strain, respectively. The dimensionless plastic strain rate  $\dot{\varepsilon}^*$  was related to the reference strain rate  $\dot{\varepsilon}_0$  by the equation

$$\dot{\varepsilon}^* = \frac{\dot{\varepsilon}}{\dot{\varepsilon}_0}, \quad (10)$$

where  $\dot{\varepsilon}_0$  is the reference strain rate, which allows a dimensionless expression in natural logarithms. Four different strain rates, including 0.0000667, 0.00667, 1.67 and 30 (1/s), were used to obtain the stress–strain curves of PP and G/PP.

The value of  $A$  was calculated from the yield strength of the experimental engineering stress–strain curve of PP and G/PP. The constants  $B$  and  $n$  were determined from the log (plastic stress) vs. log (plastic strain) plot. The constant  $C$  is the slope of dynamic/static stress ratios at 2% plastic strain vs. the natural log of the strain rate of that test. The Johnson–Cook constants for PP and G/PP are listed in Table 2. Aluminum 1050-H14 layers were also modeled by the Johnson–Cook model.

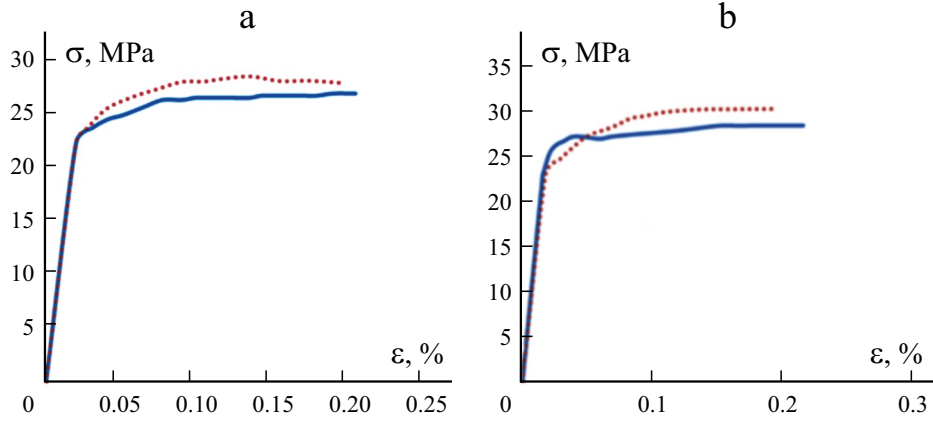


Fig. 6. A comparison of stress–strain curves  $\sigma - \varepsilon$  obtained in tensile tests of the present work with data from [18]: tensile test curves of PP (a) and G/PP (b).

The Johnson–Cook constants for aluminum are presented in Table 2. The Johnson–Cook model parameters for the nano-reinforced PP material were characterized previously in [18]. In the current study, the Johnson–Cook material constants were examined to simulate the impact behavior of aluminum, PP, and G/PP layers.

According to [2], the material parameters, including the yield strength and elastic modulus, have a high effect on the low-velocity impact behavior of multilayer structures. In Sect. 3.4, the experimental stress–strain curves of the PP and G/PP were compared against reference results [18] to characterize the identical static behavior of the materials in both studies. Therefore, it would be possible to use the material parameters of the same material in a new study too. It would be better to conduct some new experiments to clarify more about the similarity in the dynamic behavior of materials in both studies but comparing the Johnson–Cook parameters.

Experimental tensile tests according to the ASTM D638 standard were performed on PP and G/PP materials and compared against the reference results of [18]. Test specimens were prepared similar those of the PP and G/PP plates.

Figure 6 shows the stress–strain curves of the materials used in the present study and the materials in [18].

### 3.5. Material model for a Megapox™ adhesive layer

An elastic-plastic material model was considered for the adhesive layer. Tensile tests according to the ASTM D638 were carried out on Megapox™ adhesive specimens. The engineering (nominal) stress–strain curve of the Megapox epoxy adhesive is shown in Fig. 7 and was validated against the results of [23].

The true stress–strain curve of the adhesive material was calculated in some selected points by using the equations

$$\sigma_{True} = \sigma_{eng} (1 + \varepsilon_{eng}), \quad (11)$$

$$\varepsilon_{True} = \ln(1 + \varepsilon_{eng}), \quad (12)$$

where,  $\sigma_{True}$ ,  $\varepsilon_{True}$ ,  $\sigma_{eng}$ , and  $\varepsilon_{eng}$  are the true stress, true strain, engineering stress, and engineering strain, respectively [18]. Different stress and strain quantities for epoxy adhesive are presented in Table 3. The elastic material characteristics of the adhesive, including the density, elastic modulus, and Poisson ratio, were 1100 kg/m<sup>3</sup>, 0.36 GPa, and 0.4 respectively. The elastic-plastic behavior of the adhesive layer was determined by using a multilinear plasticity model according to the quantities in Table 3.

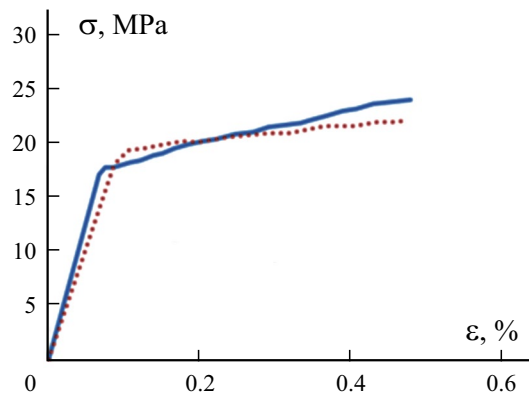


Fig. 7. Engineering stress–strain curve  $\sigma - \varepsilon$  of the Megapox adhesive.

TABLE 3. Stresses and Strains in the Megapox Epoxy Adhesive

Nominal stress, MPa	Nominal strain	True stress, MPa	True strain	Plastic strain
18	0.05	18.9	0.0488	0
20	0.1	22.0	0.0953	0.0465
21	0.2	25.2	0.1823	0.01335
22	0.3	28.6	0.2624	0.02136
24	0.4	33.6	0.3365	0.2877

### 3.6. A three-dimensional quarter model and loading conditions

The dimensions used in Sect. 3.6. were considered on the basis results of the experimental tests. Target structures with dimensions of  $18 \times 18 \times 0.68$  cm were used for modeling. To develop a three-dimensional quarter model, a square sandwich structure with an edge of 9 cm and a whole thickness of 0.68 cm was considered as the target plate on which a rigid impactor with Table 1 quantities for masses and velocities collided. The adhesive layer, the PP layer, and the aluminum layer thicknesses were 0.4, 4, and 1 mm, respectively. The adhesive and the PP or aluminum surfaces were considered to be bonded ideally. The crack propagation and adhesive separation were neglected in the model. The bonded surfaces were determined using the tie constraints in the software. The friction between the impactor and target face sheet was defined in the contact property options. A friction coefficient of 0.3 was considered for the tangential behavior. A hard contact option was chosen for the normal direction of contact. The three-dimensional quarter model of sandwich structure is illustrated in Fig. 8.

Finite-element models were developed in ABAQUS Explicit finite-element software. Linear hexahedral elements of type C3D8R were used for the sandwich target plate in the models. As shown in Fig. 8, a higher mesh density was used near the central region of the target sandwich plates to improve the accuracy of the results and to handle the highly nonlinear contact phenomenon. Furthermore, a mesh convergence was analyzed to ensure that an adequate number of elements is used in the finite-element modeling. The convergence was studied considering the effect of mesh density on the contact force and the contact duration. The thickness of each aluminum, adhesive, and PP layer was divided into 2, 6, and 8 sections, respectively. This means that, in the thickness of aluminum and PP layers, every millimeter was divided into two elements. A mesh pattern with 34,560 elements was chosen as the case with an optimum number of elements.

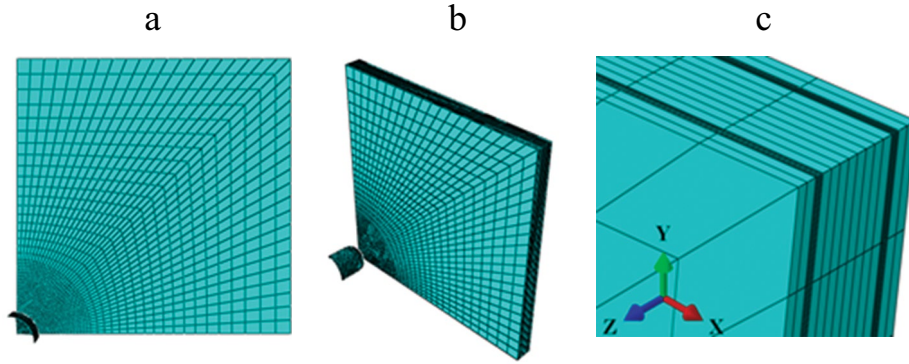


Fig. 8. Mesh details of the impactor and sandwich structure: front view (a), isometric view (b), and mesh density in the thickness (c) of the target structure.

TABLE 4. Difference Between Experimental and Numerical Results

Impact test output		Test number (linear momentum, kg·m/s)					
		1 (5.94)	2 (5.94)	3 (9.04)	4 (9.04)	5 (13.64)	6 (13.64)
Max. permanent transverse displacement of the front face, mm	Exp.	1.41	1.24	2.62	2.43	2.64	2.34
	Num. (Error%)	1.475 (4.61)	1.362 (9.84)	2.753 (5.08)	2.615 (7.61)	2.741 (3.82)	2.602 (11.19)
Max. permanent transverse displacement of the back face, mm	Exp.	0.83	0.78	2.05	1.7	2.14	1.92
	Num. (Error%)	0.7777 (-6.30)	0.7212 (-7.54)	1.863 (-9.12)	1.758 (3.41)	1.875 (-12.38)	1.779 (-7.34)
Permanent plastic radius, mm	Exp.	10.23	9.49	14.22	13.98	14.60	14.12
	Num. (Error%)	10.491 (2.55)	10.235 (7.85)	15.464 (8.75)	15.152 (8.38)	15.205 (4.14)	15.120 (7.08)
The remaining kinetic energy of impactor, J	Exp.	2.81	2.89	5.16	5.19	5.03	5.14
	Num. (Error%)	2.757 (-1.89)	2.803 (-3.01)	4.868 (-5.66)	4.899 (-5.61)	4.836 (-3.86)	4.890 (-4.86)
Peak contact force, kN	Exp.	4.16	4.51	5.48	6.04	5.50	5.82
	Num. (Error%)	4.339 (4.30)	4.709 (4.41)	5.836 (6.50)	6.138 (1.62)	5.832 (6.04)	6.017 (3.38)
Contact duration, ms	Exp.	3.74	3.71	3.78	3.54	5.75	5.49
	Num. (Error%)	3.509 (-6.18)	3.413 (-8.00)	3.533 (-6.53)	3.443 (-2.74)	5.352 (-6.92)	5.193 (-5.41)

### 3.7. Validation

The finite-element results were compared with the experimental results of Sect. 2.6. Test numbers (1, and 2), (3, and 4), and (5, and 6) were considered as the paired experiments with the same impactor characteristics, but for different core materials (pure or nanoreinforced). Accurate and clear values of impact outputs are presented in Table 4. According to the table, the difference between the numerical and the experimental results was in an acceptable range. As seen in Table 4, more remaining kinetic energies of the impactor were obtained for sandwich structures with nanoreinforced cores than with pure cores, whereas the permanent plastic radiuses smaller for the nanophased structures. The higher absorbed energy (a lower remaining kinetic energy of impactor) can be interpreted as a higher amount of damage (plastic radius) that occurred in the structure.

It can be concluded from the experimental results of the paired tests (1, 2) in Table 4 that, by introducing nanoparticles into the core of sandwich structures, without any variation in impactor characteristics, the increase of contact force and the increase of remaining kinetic energy of impactor were 8.41 and 2.85%, respectively, whereas the decrease in the contact

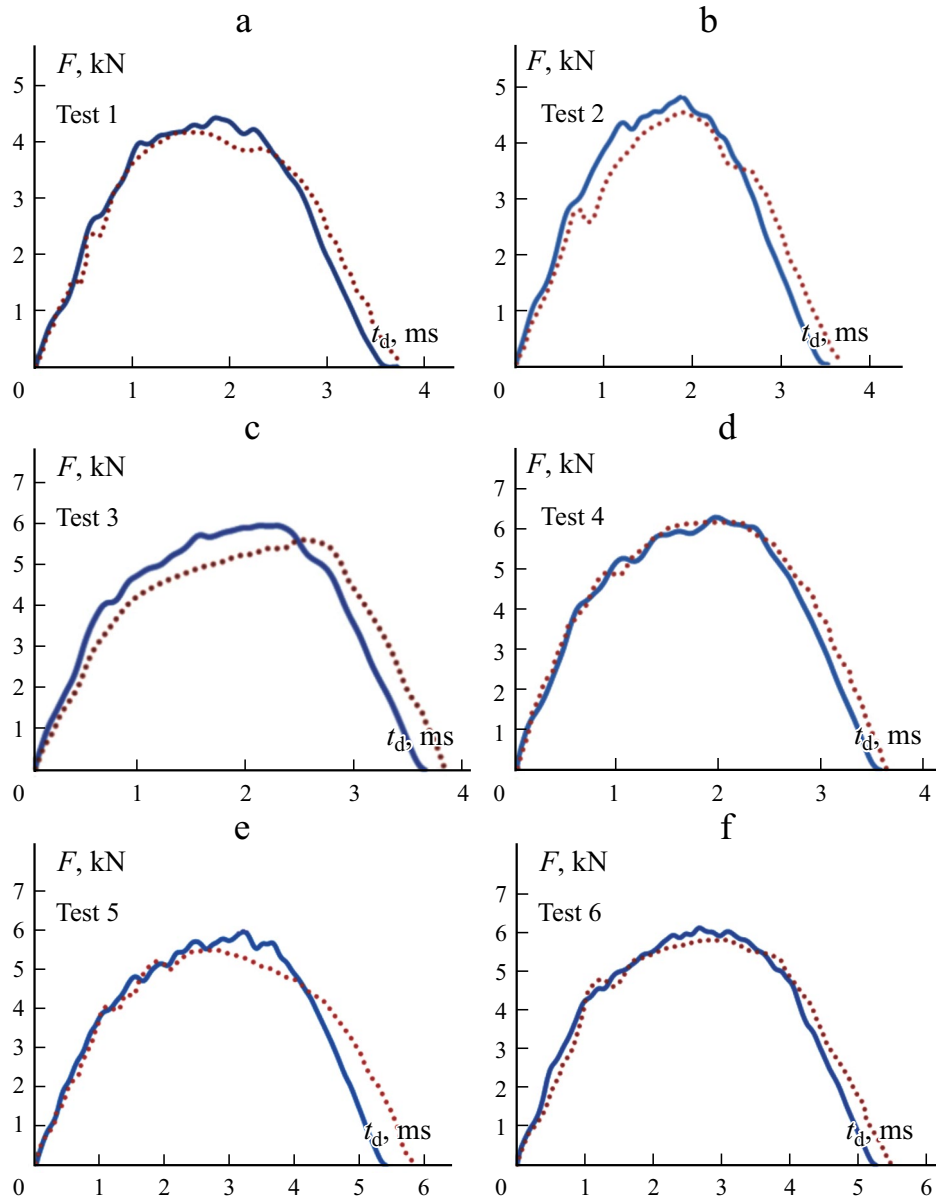


Fig. 9. A comparison between the numerical (—) and experimental (···) contact forces  $F$  versus contact duration  $t_d$  curves for different impact load conditions according to Table 1.

duration, maximum permanent transverse displacement of the front face, maximum permanent transverse displacement of the back face, and permanent plastic radius were 0.8, 12.06, 6.02, and 7.23% respectively. A similar comparison was performed for the experimental results of the paired tests (3, 4) in Table 4. The increase of contact force and the increase of remaining kinetic energy of impactor were 10.22 and 0.6%, respectively, whereas the decrease in the contact duration, maximum permanent transverse displacement of the front face, maximum permanent transverse displacement of the back face, and permanent plastic radius were 6.35, 7.25, 17.07, and 1.69% respectively. The increase in the contact force and the increase in the remaining kinetic energy of impactor in the paired tests (5, 6) were 5.82 and 2.19% respectively, whereas the decrease in the contact duration, maximum permanent transverse displacement of the front face, maximum permanent transverse displacement of the back face and permanent plastic radius were 4.52, 11.36, 10.28, and 3.29%, respectively.

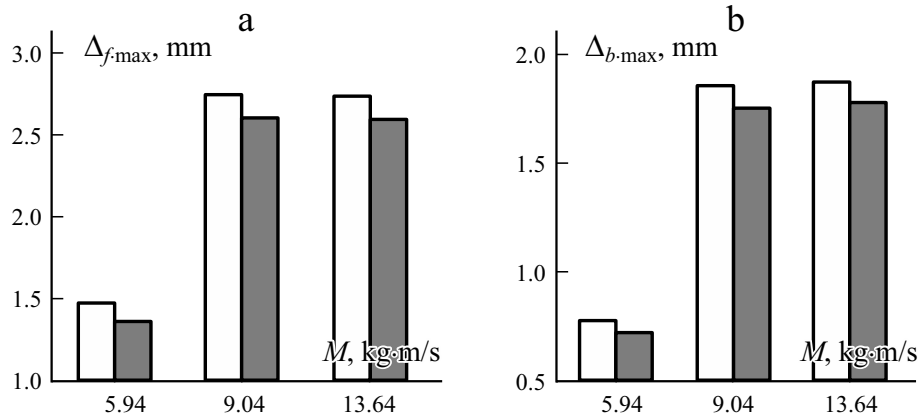


Fig. 10. The maximum permanent transverse displacement of front (□) and back (■) faces at different linear momentums  $M$ .

Figure 9 demonstrates the contact force histories of pure and nanoreinforced sandwich structures. The force–time histories were noisy for both the experimental and numerical procedures. It is common in impact tests with dynamic responses in the form of oscillations around the mean curve. An averaging scheme was applied to the force–time curves to achieve smooth results. The trend line was fitted for the experimental curves. A filter, named the ButterworthFilter, was utilized for numerical curves in the Abaqus software. The test with numbers 1, 3, and 5 were considered for sandwich structures with a pure PP core. The tests with numbers 2, 4, and 6 were considered for sandwich structures with a nano-reinforced PP core. The tests (1, 2), (3, 4), and (5, 6) were considered as paired experiments with the same impactor characteristics, but for different core materials (pure or nanoreinforced). Both numerical and experimental diagrams show that, on adding nanoparticles to the PP core, the contact force increased, but the contact time decreased. Comparing the results obtained for the tests with numbers 1 and 2 with the results obtained for the tests with numbers 3 and 4 revealed that the contact force was higher, whereas the contact duration remained nearly unchanged on increasing the impactor velocity. Comparing the results obtained for the tests with numbers 1 and 2 with the results obtained for those with the numbers 5 and 6 revealed that the contact force and contact duration increased on increasing the impactor mass.

Figure 10 shows the numerical quantities for the maximum permanent transverse displacement of the front and back faces. Comparing the results obtained for the paired experiments (1, 2) with the paired experiments (3, 4) and (5, 6) revealed that the transverse displacement enhanced on increasing the impactor velocity or impactor mass. The central transverse displacement of test number 2 was lower than that of test number 1. This means that the transverse displacement decreased by adding the graphene particles to the core of sandwich structures.

The material properties of PP, including the yield strength and the elastic modulus were changed by adding graphene to it. Therefore, the impact outputs were varied by changing the material properties, including the yield strength and elastic modulus. Increasing the yield strength or the elastic modulus of PP layers in the sandwich structures reduced the transverse displacement of the structure, causing a reduction in the contact duration. Adding nanoparticles to the PP layer reduced the plastic radius, causing an increase in the remaining kinetic energy of impactor. There existed an inverse relation between the magnitude of the contact force and transverse displacement. When the structure was deformed less in the transverse direction, the contact area between the impactor was small, and the target showed a higher contact force.

TABLE 5. Effects of Different Material Parameters of Aluminum Layers on the Maximum Permanent Transverse Displacement of the Front Face (DFF), the Maximum Permanent Transverse Displacement of the Back Face (DBF), the plastic radius (PR), the remaining kinetic energy of impactor (RKI), the contact force (CF), and the Contact Duration (CD) of “Type 1” Sandwich Structures

Material parameters of aluminum layers	DFF	DBF	PR	RKI, J	CF, kN	CD, ms
	mm					
$(E, \sigma_y, \rho)$	4.528	3.936	13.81	3.622	4.19	7.313
$(1.3E, \sigma_y, \rho)$	4.218	3.622	12.62	4.157	4.25	6.955
$(1.6E, \sigma_y, \rho)$	4.102	3.503	8.86	4.439	4.33	6.795
$(1.9E, \sigma_y, \rho)$	3.968	3.337	6.74	4.720	4.54	6.595
$(E, 1.3\sigma_y, \rho)$	3.909	3.327	11.11	4.664	4.60	7.073
$(E, 1.6\sigma_y, \rho)$	3.448	2.893	7.38	5.447	4.90	6.954
$(E, 1.9\sigma_y, \rho)$	3.079	2.593	4.41	6.073	5.14	6.834
$(E, \sigma_y, 1.3\rho)$	4.529	3.881	13.83	3.614	4.19	7.253
$(E, \sigma_y, 1.6\rho)$	4.548	3.924	13.85	3.593	4.19	7.253
$(E, \sigma_y, 1.9\rho)$	4.528	3.849	13.84	3.583	4.17	7.311

TABLE 6. Effects of Different Weight Ratios of Nanoparticles and Different Thicknesses of Aluminum and PP Layers on the Maximum Permanent Transverse Displacement of the Front Face (DFF), the Maximum Permanent Transverse Displacement of the Back Face (DBF), the Plastic Radius (PR), the Remaining Kinetic Energy of Impactor (RKI), the Contact Force (CF), and the Contact Duration (CD) of Pure and Nanoreinforced Sandwich Structures

Target structures	DFF	DBF	PR	RKI, J	CF, kN	CD, ms
	mm					
Type 1/ Pure PP core	4,528	3,936	13,81	3,622	4,19	7,313
Type 1/ 0.5% G- PP core	4,511	3,901	13,25	3,654	4,29	7,270
Type 1/ 1% G- PP core	4,529	3,934	13,65	3,632	4,19	7,302
Type 1/ 2% G- PP core	4,549	3,945	13,75	3,645	4,15	7,314
Type 2/ Pure PP core	3,653	2,959	12,31	4,254	4,73	6,595
Type 2/ 0.5% G- PP core	3,574	2,893	11,42	4,286	4,79	6,465
Type 2/ 1% G- PP core	3,622	2,926	12,15	4,248	4,69	6,534
Type 2/ 2% G- PP core	3,632	2,944	12,25	4,221	4,65	6,604
Type 3/ Pure PP core	2,445	1,643	16,30	4,830	7,15	4,916
Type 3/ 0.5% G- PP core	2,434	1,625	16,01	4,893	7,22	4,856
Type 3/ 1% G- PP core	2,442	1,635	16,15	4,836	7,14	4,916
Type 3/ 2% G- PP core	2,445	1,639	16,25	4,831	7,09	4,917

### 3.8. Effects of different mechanical and geometrical properties on the impact behavior of sandwich structures

After validation of the finite-element model assumed in Sect. 3.7., the effects of different parameters, including the thickness of the aluminum and PP layers, different weight ratio of nanoparticles, and different mechanical properties of the aluminum layers, were studied.

Three types of target structures with different thicknesses of aluminum and PP layers were considered. For Type 1 target structure, the thickness of both face sheets were 1 mm, and the PP core was considered 1-mm thick, too. For Type 2,

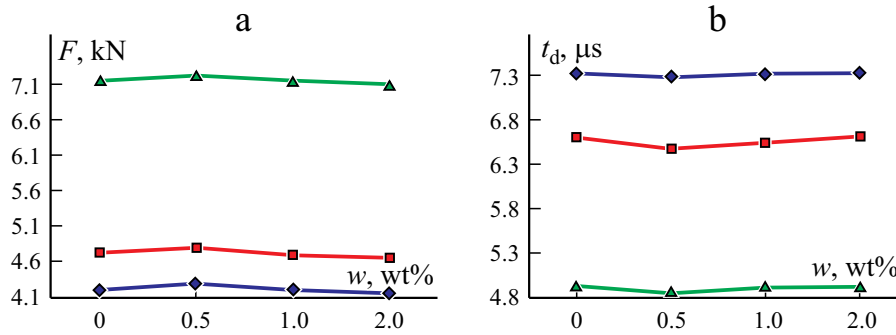


Fig. 11. Effect of different weight ratios  $w$  of graphene on impact outputs: contact force  $F$  (a) and contact duration  $t_d$  (b).

the thickness of the core was 2 mm. The aluminum face sheets were 1-mm thick. For Type 3, the thickness of the aluminum layers was 2 mm. The core thickness of Type 3 was 1 mm. The mass and velocity of the rigid impactor were equal to those in tests 5 and 6 (see Table 1).

A numerical investigation was performed to study the effects of material characteristics, including the elastic modulus, the yield strength, and the density, on the impact response of target laminates. The material characteristics did not change simultaneously. One characteristic was changed in every step to determine the effect of the parameter separately. The effects of material characteristics were studied on Type 1 structures. All the results obtained are presented in Table 5. As is seen, the displacements of target laminates, in both front and back faces, decreased at growing elastic modulus and yield strength. The elastic modulus and yield strength can change the stress–strain curve of the material directly. Therefore, the force was increased by changing these characteristics. A growth in the elastic modulus and yield strength led to a stiffer behavior target laminate, and the remaining energy reduced. The influence of density on the impact responses was not considerable.

The effects of thicknesses of aluminum and PP layers and the different weight ratios of nanoparticles are shown in Table 6. As is seen increasing the thickness of aluminum or PP layers increased the contact force, but reduced the contact duration. The transverse displacement decreased on increasing the thickness of the core or face sheets. Although the effect of different weight ratios of nanoparticles are shown in Table 6, a diagram was also plotted in Fig. 11 for a better presentation of the behavior of sandwich structures with different amounts of nanoparticles. The most important effect of adding the nanoparticles to the core material was the optimum behavior of the sandwich structures when the weight ratio of graphene platelets reached to 0.5%. In other words, by adding the graphene up to 0.5 wt% in PP material, all of the impact outputs reached to their extremum (minimum or maximum) amounts. Adding more amount of nanoplatelets up to 1 or 2 wt% did not improved the impact outputs. As an example, the contact force and the contact duration for sandwich structures with different weight ratio of nanoparticles are plotted in Fig. 11. The contact force was increased by adding 0.5% weight ratio of graphene, while the contact duration decreased. The peak and the bottom points occurred at a 0.5 wt%. After the rise or fall in 0.5 wt%, the ascending or descending trends of the curves in Fig. 11 did not continue by adding more graphene. Material properties of PP changed on adding graphene. Therefore, the impact outputs varied on changing the material properties including the yield strength and elastic modulus.

#### 4. Conclusion

For experimental tests, sandwich structures were fabricated with pure and nanoreinforced cores and aluminum face sheets. Neat and nanoreinforced cores with graphene with 0.5 wt% prepared for experimental tests. Two different core materials (pure or nanoreinforced) and three different linear momentums of the impactor were considered to study the effect of adding nanoparticles and the effect of different impactor mass and velocities on impact outputs. For the cases with the same linear



momentum of impactor, adding nanoparticles caused an increase in the contact force and remaining kinetic energy of the impactor, whereas other impact outputs, including the contact duration, dent depth, maximum permanent transverse displacement of the back face, and the damage area, decreased. All of the impact outputs enhanced on increasing the mass of impactor. All impact outputs, except the contact duration, enhanced on increasing the velocity of impactor. The impactor velocity did not influence considerably the contact duration. A good enhancement in the impact characteristics at very low graphene contents supported the efficiency of adding graphene into the polypropylene.

To further investigate the impact response of sandwich structures, a three-dimensional quarter model was developed and implemented in the ABAQUS software. The Johnson–Cook material constants characterized by the SRDM model, were examined to simulate the low-velocity impact behavior of G/PP layers. It was found that results of the finite-element analysis were in a very good agreement with experimental data. Considering the outcome of the present research, it can be stated that the proposed model with Johnson–Cook parameters is reliable enough to simulate the low-velocity impact behavior of graphene/PP nanocomposites.

After validation of the finite-element model, the effects of different parameters, including the thickness of the aluminum and PP layers, different weight ratio of nanoparticles and different mechanical properties of the aluminum layers, were investigated. Different yield strengths and elastic moduli were achieved for the core material by using different weight ratio of graphene, including pure, 0.5, 1, and 2% ones. Different yield strengths and elastic moduli were considered for aluminum layers in the finite-element modeling, too. The yield strength and the elastic modulus of the aluminum and PP layers considerably affected the impact responses of a sandwich structure, including the contact force, contact duration, the remaining kinetic energy of impactor, the plastic radius, and transverse displacements. On adding the graphene up to 0.5 wt% to the PP material, all of the impact outputs reached their extremum (minimum or maximum) amounts. Adding more graphene did not improve the impact response of the structures. The minimum amount of damage area and transverse displacement occurred in the sandwich structures with a PP/0.5% G core.

## REFERENCES

1. M. Altan, M. Bayraktar, and B. Yavuz, "Manufacturing polymer/metal macro-composite structure for vibration damping," *Int. J. Adv. Manuf. Tech.*, **86**, 2119-2126 (2016).
2. H. Khoramishad and M. Bagheri Tofighi, "Effects of mechanical and geometrical properties of adhesive and metal layers on low-velocity impact behavior of metal laminate structures," *J. Adhes. Sci. Technol.*, **29**, 592-608 (2015).
3. H. Khoramishad, M. Bagheri Tofighi, and M. Khodaei, "Effect of stacking sequence on low-velocity impact behavior of metal laminates," *Phys. Mesomech.*, **21**, 140-149 (2018).
4. A. Riccio, A. Raimondo, A. Sellitto, V. Acanfora, and M. Zarrelli, "Multifunctional polypropylene core for aerospace sandwich composite panels," *Procedia. Eng.*, **167**, 64-70 (2016).
5. M. Bulut, "Low-velocity impact tests on basalt fiber/polypropylene core honeycomb sandwich composites," *Mech. Compos. Mater.*, **56**, 121-130 (2020).
6. M. V. Hosur, A. A. Mohammed, and S. Jeelani, "Impact Response of Nanophased Polyurethane Foam Core Sandwich Composites," In: 16th International Conference on Composite Materials (ICCM-16), Kyoto, 8-13 July, 1-7, (2007).
7. M. V. Hosur, A. A. Mohammed, S. Zainuddin, and S. Jeelani, "Processing of nanoclay filled sandwich composites and their response to low-velocity impact loading," *Compos. Struct.*, **82**, 101-116 (2008).
8. M. V. Hosur, A. A. Mohammed, S. Zainuddin, and S. Jeelani, "Impact performance of nanophased foam core sandwich composites," *Mater. Sci. Eng.*, **498**, 100-109 (2008).
9. M. A. Bhuiyan, M. V. Hosur, and S. Jeelani, "Low-velocity impact response of sandwich composites with nanophased foam core and biaxial ( $\pm 45^\circ$ ) braided face sheets," *Compos. Part B-Eng.*, **40**, 561-571 (2009).
10. A. F. Avila, M. G. R. Carvalho, E. C. Dias, and D. T. L. Cruz, "Nano-structured sandwich composites response to low-velocity impact," *Compos. Struct.*, **92**, 745-751 (2010).

11. P. N. B. Reis, P. Santos, J. A. M. Ferreira, and M. O. W. Richardson, "Impact response of sandwich composites with nano-enhanced epoxy resin," *J. Reinf. Plast. Compos.*, **32**, 898-906 (2013).
12. I. Taraghi and A. Fereidoon, "Non-destructive evaluation of damage modes in nanocomposite foam-core sandwich panel subjected to low-velocity impact," *Compos. Part B-Eng.*, **103**, 51-59 (2016).
13. K. R. Ramakrishnan, S. Guerard, Z. Zhang, K. Shankar, and P. Viot, "Numerical modeling of foam-core sandwich panels with nano-reinforced composite facesheets," *J. Sandw. Struct. Mater.*, **0**, 1-26 (2019).
14. S. Feli and M. M. Jalilian, "Three dimensional solution of low velocity impact on sandwich panels with hybrid nano-composite face sheets," *Mech. Adv. Mater. Struc.*, **25**, 579-591 (2018).
15. S. Jedari Salami, "Low velocity impact response of sandwich beams with soft cores and carbon nanotube reinforced face sheets based on extended high order sandwich panel theory," *Aerosp. Sci. Technol.*, **66**, 165-176 (2017).
16. F. Vakili-Tahami, M. R. Adibeig, and S. Hassanifard, "Optimizing creep lifetime of friction stir welded PMMA pipes subjected to combined loadings using rheological model," *Polym. Test.*, **79**, 106049 (2019).
17. J. H. Ku, I. H. Jung, K. Y. Rhee, and S. J. Park, "Atmospheric pressure plasma treatment of polypropylene to improve the bonding strength of polypropylene/aluminum composites," *Compos., Part B-Eng.*, **45**, 1282-1287 (2013).
18. M. M. Shokrieh and V. Ahmadi Joneidi, "Characterization and simulation of impact behavior of graphene/polypropylene nanocomposites using a novel strain rate-dependent micromechanics model," *J. Compos. Mater.*, **49**, 2317-2328 (2014).
19. A. V. Pocius, "The electrochemistry of the FPL (Forest Products Laboratory) process and its relationship to the durability of structural adhesive bonds," *J. Adhes.*, **39**, 101-121 (1992).
20. URL: <https://imagej.nih.gov/ij/index.html> (reference date: 06.12.2021).
21. R. K. Goldberg, G. D. Roberts, and A. Gilat, "Implementation of an associative flow rule including hydrostatic stress effects into the high strain rate deformation analysis of polymer matrix composites," *J. Aerospace Eng.*, **18**, 18-27 (2005).
22. M. M. Shokrieh, R. Mosalmani, and M. J. Omid, "Strain rate dependent micromechanical modeling of reinforced polymers with carbon nanotubes," *J. Compos. Mater.*, **48**, 3381-3393 (2013).
23. Z. Emami Geiglou and T. N. Chakherlou, "Numerical and experimental investigation of the effect of the cold expansion process on the fatigue behavior of hybrid (bonded-bolted) double shear lap aluminum joints," *Int. J. Fatigue.*, **126**, 30-43 (2019).